arXiv:1612.09166v1 [cond-mat.mes-hall] 29 Dec 2016

Dynamics and decoherence in non ideal Thouless quantum motors

Lucas J. Fernández-Alcázar[1], Horacio M. Pastawski[1], and Raúl A. Bustos-Marún[1,2*]
[1] *Instituto de Física Enrique Gaviola and Facultad de Matemática Astronomía y Física, Universidad Nacional de Córdoba, Ciudad Universitaria, Córdoba, 5000, Argentina and*
[2] *Facultad de Ciencias Químicas, Universidad Nacional de Córdoba, Ciudad Universitaria, Córdoba, 5000, Argentina*

Different proposals for adiabatic quantum motors (AQMs) driven by DC currents have recently attracted considerable interest. However, the systems studied are often based on simplified models with highly ideal conditions and where the environment is neglected. Here we investigate the performance (dynamics, efficiency and output power) of a prototypical AQM, the Thouless motor. In order to correctly account for the environmental effects on this type of AQMS we extended our previous theory of decoherence in current induced forces (CIFs) to account for multiple site-dependent decoherent processes. We provide analytical expressions for the CIFs, friction coefficients and self correlation functions of the CIFs, and prove that the model is thermodynamically consistent. We find that decoherence drastically reduce the efficiency of the motor mainly due to the increase in conductance, while its effect on the output power is not so important. The effect of decoherence on the current induced friction depends on the length of the system, reducing the friction for short systems while increasing it for long ones. Finally, we find that system-lead mismatching induces additional conservative forces that alter the dynamics of the motor. In particular we show that due to this, the systems can present hysteresis and a voltage dependent switching.

PACS numbers: **07.10.Cm, 73.23.-b, 03.65.Yz.**

I. INTRODUCTION

In recent years, there has been an increasing interest in electronic transport through nanoelectromechanical systems (NEMS) where electronic degrees of freedom couple directly to the mechanical ones.[1–6] Advances in the experimental control and fabrication of NEMS[7,8] as well in the theory describing current induced forces (CIFs)[9,10] has fueled a great variety of proposals in the field such as nanocoolers, nanorefrigerators,[11–13] NEMS transistors, and nanomotors among others. An interesting example of these are the so called adiabatic quantum motors (AQMs).[14] They are nanoscopic engines driven by a flux of quantum particles and where quantum mechanics can be used for different purposes, such as boosting their efficiency for example. This class of devices works essentially as quantum pumps operated in reverse. While in a quantum pump, the periodic movement of some parameters pumps quantum particles from one reservoir to another, in a quantum motor a DC current of particles induced the cyclic motion of the device. The adjective "adiabatic" in this context refers to the limit when the dynamics of the mechanical degrees of freedom is slow compared with the dwell time of electrons passing through the device. In this regime it is commonly assumed that the mechanical degrees of freedom behave classically.

A interesting example to study the properties of AQMs is the one based on the Thouless pump.[15,16] In this system a mechanical degree of freedom couples to electrons through a periodic potential. For a large conductor, a band gap arises making the transmission of electrons forbidden withing an energy range. As previously shown, this fact can be used in the so called Thouless motor to dramatically increase the efficiency of the engine.[14] Provided that quantum interferences play a crucial role in the high performance of such systems, it is natural to wonder about the role of decoherent effects.[17,18] However, in this system decoherence events can take place anywhere along the long conductor and this should be properly taking into account. Besides that, in the ideal Thouless motor, based on a linearized Hamiltonian which also neglects the effect of the boundaries of the system, conservative forces are negligible. It is then also interesting to study first the deviations from the linearized model and then the appearance of conservative forces and its interplay with non-conservatives ones in the dynamics of the system.

In the present work, we investigate the performance in terms of dynamics, efficiency and output power, of AQMs based on the Thouless pump including decoherence and system-lead mismatching in a tight binding description of the system. In section II we present the theoretical framework used to describe the dynamics of mechanical systems subject to current induced forces in presence of decoherence. In subsection II A we extend our previous theory of CIFs in presence of decoherence to account for multiple site-dependent decoherent processes. In subsection II B we specify the models used to describe the Thouless motor and define its efficiency and output power. The main results are discussed in section III. In subsection III A we study the deviations of Thouless motors with respect to their ideal description. In subsection III B we discuss the interplay of conservative and non-conservative forces in the dynamics of the system. Finally, in subsection III C we investigate the effect of decoherence on the performance of these AQMs.

II. THEORY

Langevin Dynamics - In this work we will treat the mechanical degrees of freedom of the system as classical fields acting on the electrons, treated as quantum spinless non-interacting particles, where the dynamics of the classical fields are assumed slow compared to that of the electrons. In this context of mechanical modes embedded in an electronic environment, it is natural to describe the dynamics of the classical system by a set coupled Langevin equations,

$$M_\nu \ddot{x}_\nu + \frac{\partial U}{\partial x_\nu} = F_\nu - \sum_{\nu'} \gamma_{\nu,\nu'} \dot{x}_{\nu'} + \xi_\nu, \tag{1}$$

where in the left hand side M_ν is the mass associated with coordinate x_ν, and dU/dx_ν accounts for any force not included in the right hand side of the equation, which could be external forces or even internal forces but not classifiable as CIFs. The right hand side of eq. 1 accounts for the CIFs[9] where F is the mean adiabatic reaction force, the coefficients $\gamma_{\nu,\nu'}$ are associated with dissipative friction forces, for $\nu = \nu'$, and effective "Lorentz" forces, for $\nu \neq \nu'$, while ξ_ν accounts for the force fluctuations. All these terms have a quantum origin and expressions in terms of scattering matrices or Green functions are given in Refs.[9,19]. The mean adiabatic reaction force can be written as

$$F_\nu = \sum_\alpha \int \frac{d\varepsilon}{2\pi \mathrm{i}} f_\alpha \left(S^\dagger \frac{\partial S}{\partial x_\nu} \right)_{\alpha,\alpha}, \tag{2}$$

where S is the scattering matrix and f_α is the Fermi function of the conduction mode or channel α associated with some lead with chemical potential μ_α. We will be interested only in the first order expansion of CIFs close to equilibrium. Then, it is enough to consider only the equilibrium contribution to γ, which is given by[19]

$$\gamma^{eq}_{\nu,\nu'} = \frac{1}{2} \int \frac{d\varepsilon}{2\pi} \frac{\partial f}{\partial \varepsilon} \sum_{\alpha,\beta} \left(S^\dagger \frac{\partial S}{\partial x_\nu} \right)_{\alpha,\beta} \left(S^\dagger \frac{\partial S}{\partial x_{\nu'}} \right)_{\beta,\alpha} \tag{3}$$

where f is the equilibrium Fermi function. Provided that electronic fluctuations happen at short time scales, ξ_ν is locally correlated in time and its variance $D_{\nu,\nu'}$ can be written as $\langle \xi_\nu(t) \xi_{\nu'}(t') \rangle \approx D_{\nu,\nu'} \delta(t-t')$, where its equilibrium value is given by

$$D_{\nu,\nu'} = 2kT \gamma^{eq}_{\nu,\nu'} \tag{4}$$

Current - Suppose a system is connected to an arbitrary number of conduction channels α with chemical potential μ_α and subject to the movement of an arbitrary number of classical degrees of freedom x_ν coupled somehow to the electronic degrees of freedom. The total current at channel α, in the adiabatic limit respect to the movement of the (x_ν)s, in the low bias regime, and for non-interacting particles, can be evaluated by

$$I_\alpha = I^{bias}_\alpha + I^{pump}_\alpha + \delta I_\alpha, \tag{5}$$

where I^{bias}_α is the bias current consequence of the chemical potential differences among the channels, I^{pump}_α is the pumped current consequence of the adiabatic movement of the classical degrees of freedom, and δI_α is the noise in the current.

The bias current at channel α is given by[20,21]

$$I^{bias}_\alpha = -\frac{e}{h} \sum_\beta T_{\alpha\beta} \delta\mu_\beta, \tag{6}$$

where e is the electron charge, h the Planck constant, $T_{\alpha\beta}$ is the probability of transmission between channels α and β, which represents an adimensional conductance[22], $T_{\alpha\alpha} = -\sum_{\beta\neq\alpha} T_{\alpha\beta}$, and $\delta\mu_\beta = \mu_\beta - \mu_0$ with μ_0 being the equilibrium chemical potential. Note that we are not including the factor 2 in the current as we are considering that electrons with different spins belongs to different conduction channels of the same lead.

The pumped current at channel α can be evaluated by[23,24]

$$I^{pump}_\alpha = e \sum\nolimits_\nu \frac{\mathrm{d}n_\alpha}{\mathrm{d}x_\nu} \dot{x}_\nu, \tag{7}$$

where dn_α/dx_ν is the emittance of channel α due to a chance in the parameter x_ν.[25] At equilibrium it can be evaluated from

$$\frac{\mathrm{d}n_\alpha}{\mathrm{d}x_\nu} = \int \frac{d\varepsilon}{2\pi \mathrm{i}} \left(-\frac{\partial f}{\partial \varepsilon} \right) \left(\frac{\partial S}{\partial x_\nu} S^\dagger \right)_{\alpha,\alpha}, \tag{8}$$

Deviations from the mean current given by δI_α are provided by thermal (or Johnson–Nyquist) and shot noise.[26] It is assumed that it consists of rapid fluctuations of the current where its current-current correlations are given by $\left\langle \delta\vec{I}_\alpha(t-t') \delta\vec{I}_\beta(t') \right\rangle = D^{(I)}_{\alpha,\beta}\ \delta(t-t')$. The shot noise contribution to δI_α vanishes at equilibrium but thermal noise remains resulting in[26]

$$D^{(I)}_{\alpha,\beta} = -2k_B T \frac{e^2}{h} T_{\alpha\beta}, \tag{9}$$

where $k_B T$ is the thermal energy.

Decoherence - The type of decoherence modeled in this work considers that electrons are removed with a certain probability of the system and then reinjected into a given site i with a random phase.[27–30] As first noticed by Büttiker,[20] this is equivalent to the effect of a voltmeter measuring the site i in the low bias limit. Voltmeters are modeled by leads attached to specific sites where the particle number conservation, i.e. $I_{\phi,i} = 0$, is ensured by a chemical potential $\mu_{\phi,i}$ tuned for such a purpose. The rate of decoherent events, $1/\tau_\phi = 2\Gamma_{\phi,i}/\hbar$, given in the model by the imaginary part of the self energy of the coupling to the fictitious probes, $\Gamma_{\phi,i}$, was formally identified by D'Amato and Pastawski[27,28,31] with the rate of escape of electrons to a bigger Hilbert's space that accounts for the interaction of electrons with phonons or other processes not included in the original Hamiltonian. The advantage of this identification is that the values of $(\Gamma_{\phi,i})$s

can be estimated from the Hamiltonian formulation of the complete problem.[32] In the linear response regime the energy of the electron is preserved but not its momentum which leads, in the limit of high decoherence rate, to a random-walk-like dynamic for long conductors. This, in turn, provides the correct asymptotic limit for large conductors compatible with Ohm's law, $I \propto L^{-1}$ where L is the length of the system[27,28,31]. Note that this can be used to estimate the value of $\Gamma_{\phi,i}$ for real systems.[32] Direct comparison with numerical simulations also showed that the type of decoherence modeled is equivalent to the effect of fast random fluctuations of local energies given by a classical field.[30]

In a previous work we extended the above method to account for decoherence in CIFs.[17] The key in that case was to take into account all the terms of the current in eq. 5 which results in a model consistent with the positivity of friction coefficients in equilibrium, Onsager reciprocity relations, as well as the fluctuation-dissipation theorem. This self-consistency of the model is fundamental otherwise the resulting dynamics could produce unphysical results. In the following we will further extend the method, originally formulated for a two channel system of zero dimension, to include decoherence into a wider class of systems, connected to an arbitrary large number of reservoirs and subject to multiple site-dependent decoherent processes.

A. Current and current induced forces for multiple site-dependent decoherent processes

Currents - In what follows, we will make a distinction between the real conduction channels and fictitious probes labeling them as ℓ and ϕ respectively. In this notation, the vector containing the total current at each channel, $\vec{I} = \left(\vec{I}_\ell \ , \ \vec{I}_\phi\right)^T$, results

$$\begin{pmatrix} \vec{I}_\ell \\ \mathbf{0} \end{pmatrix} = -\frac{e}{h}\begin{pmatrix} \mathbb{T}_{\ell\ell} & \mathbb{T}_{\ell\phi} \\ \mathbb{T}_{\phi\ell} & \mathbb{T}_{\phi\phi} \end{pmatrix}\begin{pmatrix} \delta\vec{\mu}_\ell \\ \delta\vec{\mu}_\phi \end{pmatrix} + e\sum\nolimits_\nu \begin{pmatrix} \mathrm{d}\vec{n}_\ell/\mathrm{d}x_\nu \\ \mathrm{d}\vec{n}_\phi/\mathrm{d}x_\nu \end{pmatrix}\dot{x}_\nu + \begin{pmatrix} \delta\vec{I}_\ell \\ \delta\vec{I}_\phi \end{pmatrix}. \quad (10)$$

where we have used eqs. from 5 to 8, and included the null current condition through fictitious leads $\vec{I}_\phi \equiv 0$.[18,33] Solving this equation by blocks, we obtain the $\delta\vec{\mu}_\phi$ that satisfy charge conservation,

$$\begin{aligned}\delta\vec{\mu}_\phi &= \delta\vec{\mu}_\phi^{\,neq} + \delta\vec{\mu}_\phi^{\,pump} + \delta\vec{\mu}_\phi^{\,fluc} \\ &= \left(-\mathbb{T}_{\phi\phi}\right)^{-1}\mathbb{T}_{\phi\ell}\ \delta\vec{\mu}_\ell \\ &\quad -\sum\nolimits_\nu h\left(-\mathbb{T}_{\phi\phi}\right)^{-1}\frac{\mathrm{d}\vec{n}_\phi}{\mathrm{d}x_\nu}\dot{x}_\nu \\ &\quad -\frac{h}{e}\left(-\mathbb{T}_{\phi\phi}\right)^{-1}\delta\vec{I}_\phi. \end{aligned} \quad (11)$$

We consider that the last term $\delta\vec{\mu}_\phi^{\,fluc}$ fluctuates with a time scale fast compared with that of the mechanical degrees of freedom. Replacing $\delta\vec{\mu}_\phi$ into eq. 10 we obtain the expression for the electronic currents corrected by decoherent processes,

$$\begin{aligned}\vec{I}_\ell = &-\frac{e}{h}\left\{\mathbb{T}_{\ell\ell} + \mathbb{T}_{\ell\phi}\left(-\mathbb{T}_{\phi\phi}\right)^{-1}\mathbb{T}_{\phi\ell}\right\}\delta\vec{\mu}_\ell \\ &+e\sum\nolimits_\nu\left\{\frac{\mathrm{d}\vec{n}_\ell}{\mathrm{d}x_\nu} + \mathbb{T}_{\ell\phi}\left(-\mathbb{T}_{\phi\phi}\right)^{-1}\frac{\mathrm{d}\vec{n}_\phi}{\mathrm{d}x_\nu}\right\}\dot{x}_\nu \\ &+\delta\vec{I}_\ell + \mathbb{T}_{\ell\phi}\left(-\mathbb{T}_{\phi\phi}\right)^{-1}\delta\vec{I}_\phi. \end{aligned} \quad (12)$$

The first term is the total non-equilibrium current including decoherence, also derived in ref.[18]. The second one is the pumped current in presence of decoherence which result in an extension to multiple site-dependent decoherent processes of the expression derived in refs.[34,35]. Finally, the third term of eq. 12 are the currents fluctuations due thermal noise and can be evaluated using eq. 9.

Current induced forces - We start by splitting the Fermi function as $f_\alpha = f + \Delta f_\alpha$. Then, the force can be expressed as

$$F_\nu = F_\nu^{eq} + \Delta F_\nu. \quad (13)$$

The equilibrium force F_ν^{eq}, which is conservative, is given by

$$\vec{F}^{eq} = -\nabla U^{eq}, \quad (14)$$

where

$$U^{eq} = -\int \frac{\mathrm{d}\varepsilon}{2\pi\mathrm{i}} f \,\mathrm{Tr}\left(\ln S\right). \quad (15)$$

The other term of the force, ΔF_ν, results

$$\Delta F_\nu = \sum_\alpha \int \frac{\mathrm{d}\varepsilon}{2\pi\mathrm{i}}\Delta f_\alpha \left(S^\dagger \frac{\partial S}{\partial x_\nu}\right)_{\alpha,\alpha}. \quad (16)$$

Taking the low temperatures and small bias limits, one can rewrite eq. 16 as

$$\Delta F_\nu = \left(\frac{\mathrm{d}\vec{n}^{(*)}}{\mathrm{d}x_\nu}\right)^T \cdot \delta\vec{\mu} \quad (17)$$

where $\mathrm{d}\vec{n}^{(*)}/\mathrm{d}x_\nu = (\mathrm{d}\vec{n}_\ell^{(*)}/\mathrm{d}x_\nu \ , \ \mathrm{d}\vec{n}_\phi^{(*)}/\mathrm{d}x_\nu)^T$, $\delta\vec{\mu} = (\delta\vec{\mu}_\ell, \delta\vec{\mu}_\phi)^T$, and the injectance[25] $(\mathrm{d}\vec{n}^{(*)}/\mathrm{d}x_\nu)$, is given by

$$\begin{aligned}\frac{\mathrm{d}n_\alpha^{(*)}}{\mathrm{d}x_\nu}(\vec{B}) &= \int \frac{\mathrm{d}\varepsilon}{2\pi\mathrm{i}}\left(-\frac{\partial f}{\partial\varepsilon}\right)\left(S^\dagger(\vec{B})\frac{\partial S(\vec{B})}{\partial x_\nu}\right)_{\alpha,\alpha} \\ &= \frac{\mathrm{d}n_\alpha}{\mathrm{d}x_\nu}(-\vec{B}). \end{aligned} \quad (18)$$

where $\vec{B}$ represents some external magnetic fields. In the last step we used the reciprocity relation $S_{\alpha,\beta}(\vec{B}) = S_{\beta,\alpha}(-\vec{B})$, which is a consequence of particle conservation, $S^\dagger S = \mathbb{I}$, and time reversal for spinless particles $S(-\vec{B})S^*(\vec{B}) = \mathbb{I}$.[36]

By replacing $\delta\vec{\mu}_\phi$ from eq. 11 in eq. 17, we obtain

$$\Delta F_\nu = F_\nu^{ne} - \sum\nolimits_{\nu'} \gamma^\phi_{\nu\nu'}\dot{x}_{\nu'} + \xi_{\phi,\nu}. \tag{19}$$

where the first term represent the non equilibrium forces, the second the dissipative forces induced by decoherence, and the third the force fluctuations induced by decoherence. These last two terms add to the dissipative forces and force fluctuations already present in the system, eqs. 3 and 4.

The non-equilibrium forces are

$$F_\nu^{ne} = \left\{ \frac{\mathrm{d}\vec{n}_\ell^{(*)}}{\mathrm{d}x_\nu} + \left(\frac{\mathrm{d}\vec{n}_\phi^{(*)}}{\mathrm{d}x_\nu}\right)^T \left(-\mathbb{T}_{\phi\phi}\right)^{-1} \mathbb{T}_{\phi\ell} \right\} \delta\vec{\mu}_\ell. \tag{20}$$

These forces are not necessarily conservative and, as we will see later, they are related to the pumped currents, eq. 26.

The coefficients of the decoherence induced dissipative forces $\gamma^\phi_{\nu\nu'}$, are given by

$$\gamma^\phi_{\nu\nu'} = h \left(\frac{\mathrm{d}\vec{n}_\phi^{(*)}}{\mathrm{d}x_\nu}\right)^T \left(-\mathbb{T}_{\phi\phi}\right)^{-1} \frac{\mathrm{d}\vec{n}_\phi}{\mathrm{d}x_{\nu'}}. \tag{21}$$

It can be proved that the matrix γ^ϕ, whose elements are $\gamma^\phi_{\nu\nu'}$, is positive definite in our case, spinless particles in the absence of magnetic fields, see Appendix A.

Finally, the third term of eq. 19 are the decoherence induced fluctuating forces which are characterized by its self-correlation $\langle \xi_{\phi,\nu}(t)\xi_{\phi,\nu'}(t')\rangle = D^\phi_{\nu\nu'}\delta(t-t')$, where

$$D^\phi_{\nu\nu'} = \frac{h^2}{e^2} \left(\frac{\mathrm{d}\vec{n}_\phi^{(*)}}{\mathrm{d}x_\nu}\right)^T \left(-\mathbb{T}_{\phi\phi}\right)^{-1} \times \left\langle \delta\vec{I}_\phi \otimes \delta\vec{I}_\phi \right\rangle \left[\left(-\mathbb{T}_{\phi\phi}\right)^{-1}\right]^T \frac{\mathrm{d}\vec{n}_\phi^{(*)}}{\mathrm{d}x_{\nu'}} \tag{22}$$

In the absence of external magnetic fields and assuming near equilibrium conditions, using eq. 9, one arrives to the fluctuation-dissipation relation of decoherence induced γ's and ξ's

$$D^\phi_{\nu\nu'} = 2k_B T\ \gamma^\phi_{\nu\nu'}, \tag{23}$$

Now, let us average over ensembles the quantities in eqs. 12 and 19 in order to make fluctuating terms zero. Then, we can put those equations in the form

$$\begin{pmatrix} -\overrightarrow{F} \\ \overrightarrow{I} \end{pmatrix} = \begin{pmatrix} -\overrightarrow{F}^{eq} \\ \overrightarrow{I}^{eq} \end{pmatrix} + \begin{pmatrix} \mathbb{L}_{11} & \mathbb{L}_{12} \\ \mathbb{L}_{21} & \mathbb{L}_{22} \end{pmatrix} \begin{pmatrix} \overrightarrow{\dot{x}} \\ \overrightarrow{\delta\mu} \end{pmatrix}. \tag{24}$$

We can consider the forces $\overrightarrow{F}$ and the currents $\overrightarrow{I}$ as generalized fluxes and velocities $\overrightarrow{\dot{x}}$ and chemical potentials $\overrightarrow{\delta\mu}$ as generalized forces in a thermodynamic sense. The coefficients $\mathbb{L}_{12}$ and $\mathbb{L}_{21}$ can be identified with Onsager's coefficients, which in our system should accomplish $\mathbb{L}_{\nu\alpha}(\vec{B}) = -\mathbb{L}_{\alpha\nu}(-\vec{B})$, see ref.[37,38]. This can be readily verified in eqs. 12 and 20

$$\left.\frac{\partial F_\nu}{\partial\left(\delta\mu_\alpha\right)}\right|_{eq,\vec{B}} = -\mathbb{L}_{\nu,\alpha}(\vec{B}) = \mathbb{L}_{\alpha,\nu}(-\vec{B}) = \left.\frac{\partial I_\alpha}{\partial\dot{x}_\nu}\right|_{eq,-\vec{B}}. \tag{25}$$

When an integral over the motor's cycle is performed, we obtain

$$W = \vec{N}\cdot\delta\vec{\mu}, \tag{26}$$

where W is the work per cycle performed by CIFs for an infinitesimally slow motion and in the low bias limit. The vector $\vec{N}$ contains the number of particles pumped per cycle over each conduction channel. This expression, which essentially reflects energy conservation, can be seen as the generalization of similar relations discussed in previous works[14,17,37] to multi-channel systems with multiple site-dependent decoherent processes.

Finally, one can check that the model is consistent with the second law of thermodynamics. As shown in ref.[39] the rate of entropy production $\dot{S}^{diss}$ for driven quantum electronic systems is

$$T\dot{S}^{diss} = -\left(\vec{F} - \vec{F}^{eq}\right)\cdot\dot{\vec{x}} + \frac{1}{e}\vec{I}\cdot\delta\vec{\mu}. \tag{27}$$

In our case, this results

$$T\dot{S}^{diss} = \vec{\dot{x}}^T\left(\gamma^{eq} + \gamma^\phi\right)\vec{\dot{x}} + \vec{\delta\mu}^T\left(-\frac{e}{\hbar}\mathbb{T}\right)\vec{\delta\mu} + \sum_{\alpha\nu}\left(\frac{\mathrm{d}n_\alpha}{\mathrm{d}x_\nu} - \frac{\mathrm{d}n_\alpha^{(*)}}{\mathrm{d}x_\nu}\right)\delta\mu_\alpha\dot{x}_\nu. \tag{28}$$

Using 3, 21, and 25, together with Appendix A one can readily check that for the case of interest, spinless particles in the absence of magnetic fields, the rate of entropy production $\dot{S}^{diss}$ is always positive.

B. Thouless quantum motor

Tight binding model - A Thouless quantum motor is basically the reverse of a Thouless pump. In principle, this can be accomplished in several ways. One possible realization of it is schematized in fig. 1. In our proposal the Thouless motor consists of just a conducting wire, which could be a conducting polymer for example, coiled around a rotational piece with periodically arranged charges on its surface. For simplicity in the following we will consider a single-channel wire where the potential of the conduction electrons traversing the wire is given by

$$U(x) = 2\Delta\cos(2\pi x/\lambda - \theta). \tag{29}$$

Here Δ is the coupling strength with the classical coordinate, λ is the period and θ varies according to the

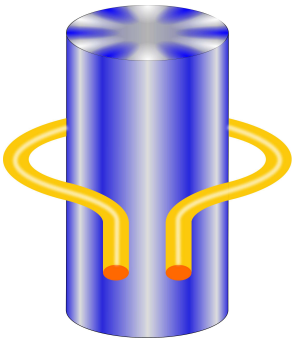

FIG. 1. Scheme of a possible Thouless motor made out of charges periodically arranged in the surface of a rotational piece and interact with a wire coiled around it. Rotation of the cylinder changes the potential sensed by the electrons in the wire.

angular position of the rotor. The mechanical rotation is described uniquely by the coordinate θ, which we assume slow respect to the dwell time of the electrons inside the wire. The dynamics of the rotor will be described by the angular Langevin equation

$$M_\theta \ddot{\theta} = F_\theta - \gamma_\theta \dot{\theta} + \xi_\theta. \tag{30}$$

Here M_θ is the moment of inertia of the rotor, F_θ is the mean adiabatic reaction force which is a torque in the present case, $\gamma_\theta \dot{\theta}$ is the friction force where γ_θ is the friction coefficient in units of "Energy $\times$ time/radians^2", and ξ_θ is the noise component of the CIFs, also a torque.

In order to calculate all the terms of the CIFs, we will resort to a tight-binding model. The Hamiltonian of electrons inside the wire is

$$\hat{H}_S = \sum_{n=1}^{N} \left\{ E_n \hat{c}_n^\dagger \hat{c}_n - V_0 \left[\hat{c}_n^\dagger \hat{c}_{n-1} + \hat{c}_{n-1}^\dagger \hat{c}_n \right] \right\}, \tag{31}$$

where $\hat{c}_n^\dagger$ and $\hat{c}_n$ are the creation and annihilator operators at site n, V_0 is the hopping, and $E_n = U(x)$ is the site energy, being $x = na$ with a the net constant and n the site index. We will include the leads through self energies, Σ, acting on the first and last sites, 1 and M, where

$$\Sigma(\varepsilon) = \lim_{\eta \to 0^+} \frac{\varepsilon + \mathrm{i}\eta}{2} - \mathrm{sgn}(\varepsilon) \sqrt{\left(\frac{\varepsilon + \mathrm{i}\eta}{2} \right)^2 - V_0^2}. \tag{32}$$

Then, the total effective Hamiltonian results

$$\hat{H}_{eff} = \hat{H}_S + \Sigma(\varepsilon)[\hat{c}_1^\dagger \hat{c}_1 + \hat{c}_M^\dagger \hat{c}_M]. \tag{33}$$

Note that with this Hamiltonian there is a jump in the site energies E_n between the leads and the system. Such abrupt change of the potential energy can cause the scattering of the incoming and/or outgoing wave functions which in turn may affect CIFs. This effect, not previously discussed for AQMs, should be present in almost any device acting as a AQM and, as will discuss in the next section, it can dramatically affect the dynamics of the system.

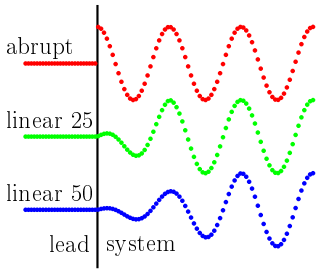

FIG. 2. Scheme showing how the site energies changes for different type of system-lead transitions. See section II B, *Tight binding model*.

In order to account for different system-lead junctions we used a linear function $f(n)$ that multiply the site energies E_n of the M_l firsts and lasts sites. The term "linear M_l" in the figures will stand for $f(x) = x/M_l$, where $x = n$ or $x = M_l - n$ for the first or last sites respectively. In this way the larger the M_l the smoother the lead-system transition, the "abrupt" transition correspond to $M_l = 1$, see fig. 2. The total size of the system considered is 2000 sites and the period λ is 25 sites. For simplicity in all calculation we assume spinless particles and single channel leads.

Ideal model - The Thouless motor has been studied previously using what we call here the ideal model. In this model the Hamiltonian is linearized respect to the momentum of the electrons, resulting in an effective Hamiltonian with counter propagating linear channels and backscattering due to the periodic potential,

$$\hat{H} = v_F p \sigma^z + \Delta \left(\sigma^x \cos\theta + \sigma^y \sin\theta \right) \Theta(L/2 - |x|). \tag{34}$$

Here L is the length of the system, Θ is the step function, the momenta are measured from $\pm k_0$ and energies from $\hbar^2 k_0^2/2m$ with $k_0 = \pi/a$, the (σ^i)s denote the Pauli matrices in the space of the counter propagating channels, and the real electron spin is not included for simplicity. Using this Hamiltonian and assuming a perfect system-lead matching one can solve analytically the scattering matrix and its derivatives for the Thouless motor. In the limit $L \to \infty$ and for electron's energies withing the band gap, one finds that the charge pumped per cycle and the efficiency are one while the equilibrium forces and the transmittance are zero.[14]

Work and efficiency - In order to avoid confusions we will define some magnitudes in the stationary regime that will be discussed in the following sections. The adiabatic work of CIFs, $\lim_{\dot{\theta} \to 0} W = W^{(a)}(\theta)$, is

$$W^{(a)}(\theta) = \int_0^\theta F(\theta') d\theta'. \tag{35}$$

The total work per cycle $W^{(\text{total})}$ of the system is

$$W^{(\text{total})} = W^{(a)} - W^{(load)} - \int_0^\tau \gamma(t')\dot{\theta}^2 dt', \qquad (36)$$

where $W^{(load)}$ is the work exerted by some external force against which one wants to move the system, and τ is the period of the motor. The output power per cycle $\dot{W}^{(\text{load})}$ can be obtained from the steady state condition $W^{(\text{total})} = 0$, while the input power is simply the total current times the the applied voltage. Then, the thermodynamic efficiency, calculated as the average output power per cycle over the average input power per cycle, results

$$\eta_{TD} = \frac{N\delta\mu - \int_0^\tau \gamma(t')\dot{\theta}^2 dt'}{\tau \langle T_{LR}\rangle \delta\mu^2 + N\delta\mu}, \qquad (37)$$

where we have used eq. 26, assumed a two leads system with an arbitrary number of conduction channels, $\langle T_{LR}\rangle$ is sum of the average transmittances (averaged over time) that connects all channels of one lead with all channels of the other, N is the total charge pumped per cycle to one lead through any channel of it, and $\delta\mu = |\mu_L - \mu_R|$ is the chemical potential difference among the leads.

The evaluation of η_{TD} requires the integration of the equation of motion of the problem. However, this problem can be circumvented by assuming a terminal velocity approximately constant. Then, the thermodynamic efficiency results

$$\eta_{TD} \approx \frac{N - 4\pi^2 \langle\gamma\rangle / (\tau\delta\mu)}{\tau \langle T_{LR}\rangle \delta\mu + N}. \qquad (38)$$

where $\langle\gamma\rangle$ is the average friction coefficient, and the value of τ is left as a free parameter which depends ultimately on $W^{(\text{load})}$

$$\tau \approx 4\pi^2 \frac{\langle\gamma\rangle}{N\delta\mu - W^{(\text{load})}}, \qquad (39)$$

assuming $F^{(\text{load})}(\theta)$ independent of $\dot{\theta}$ and thus independent of τ, or

$$\tau \approx 4\pi^2 \frac{\langle\gamma + \gamma^{(\text{load})}\rangle}{N\delta\mu}, \qquad (40)$$

assuming $F^{(\text{load})}(\theta)$ proportional to $\dot{\theta}$.

Taking $\dot{\theta}$ constant results a good approximation for large momentum of inertia in the steady state as shown in Appendix B of ref.[17] and in panel C of fig 6. This approximation will be used in figs. 8 and 9 of the next section.

III. RESULTS

The Thouless motor has shown to be an optimal candidate for the realization of an AQM since its maximum theoretical efficiency is one.[14] In this section we will evaluate its performance under non ideal conditions such as non-linear dispersion relations of the Hamiltonian, non-ideal system-lead matchings, external friction sources, and decoherence of the electrons responsible of the motor's motion.

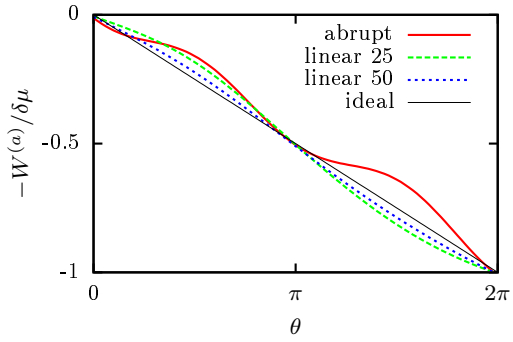

FIG. 3. Effect of the border conditions on the adiabatic work $W^{(a)}$. The line labeled 'ideal' correspond to the expected result from the ideal model. $W^{(\text{load})} = 0$, $\varepsilon = 0$, $\Delta = 0.001V_0$, $\delta\mu = 10^{-4}V_0$, $\lambda = 25a$

A. Deviations from the ideal model

The proposal of Thouless motors given in Ref.[14] involve several simplifications in order to obtain an analytic solution of the CIFs. One of this simplification involves neglecting the scattering of electrons entering the system. However giving that the potential profile inside the system is periodic and changes with the coordinate of the mechanical degree of freedom while the potential profile in the leads is constant and fixed, there must be a finite θ-dependent scattering of electrons entering and leaving the sample. Therefore, CIFs must be affected by the details of the junctions. It is worth to mention than this effect prevails at equilibrium ($\delta\mu = 0$) and is a consequence of the quantum nature of the particles driving the motion of the system. Fig. 3 shows an example of the emergence of corrections to the CIFs in the Thouless motor as consequence of the "edge mismatching". There, the work performed as function of the coordinate shows oscillations that decrease with the softening of the system-lead transition. The strength of this edge effect will depend of course on the details of the system-lead transition but also on the coupling strength Δ as can be seen in fig 4. According to this figure one way to reduce this edge mismatching is to reduce the coupling strength Δ. However, this can not be done without consequences as it is always necessary a gap that makes the transmittance zero and drives the efficiency towards one. For this reason a smaller value of Δ will require a larger wire, which could bring its own consequences such as decoherence.

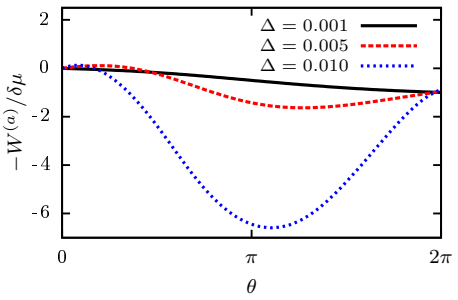

FIG. 4. Effect of Δ (in units of V_0) on the adiabatic work $W^{(a)}$. $W^{(\mathrm{load})} = 0$, $\varepsilon = 0$, $\delta\mu = 10^{-4}V_0$, $\lambda = 25a$, and border condition "linear 25".

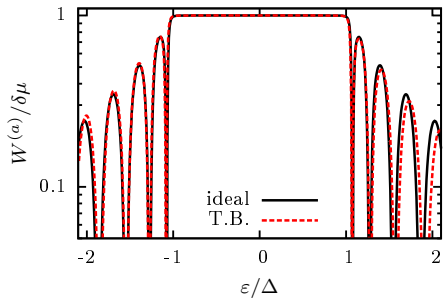

FIG. 5. Comparison of the adiabatic work $W^{(a)}$ per cycle calculated from the tight binding model (T.B.) and the ideal model (ideal). Fermi energy ε measured from the center of the band gap, $W^{(\mathrm{load})} = 0$, $\Delta = 0.001V_0$, $\delta\mu = 10^{-4}V_0$, $\lambda = 25a$, and border condition "linear 25".

Taking into account that the ideal model of the Thouless motor is based on a linearized Hamiltonian, it is expected some deviations of the results respect to the energy of the electrons, specially at energies far from the center of the band gap. However, as can be seen in fig. 5 the differences are not significant, at least at small values of the coupling strength Δ.

B. Dynamics

One of the key parameters that affect the dynamics of the studied system is the friction coefficient γ. In realistic situations dissipation of the mechanical energy can arise from different sources not only from the CIFs. Therefore, there is in principle a minimal value of γ, that arising from CIFs, but not a maximum one. In order to study the effect on the dynamics of different parameters, we solved the equation of motion of Thouless motors using eq. 30 for a wide range of different conditions. The results are summarized in the phase diagram shown in fig. 6. In the calculations we take for simplicity γ as constant, an arbitrary moment of inertia $M_\theta = 1000\hbar^2/(V_0\mathrm{rad}^2)$, and

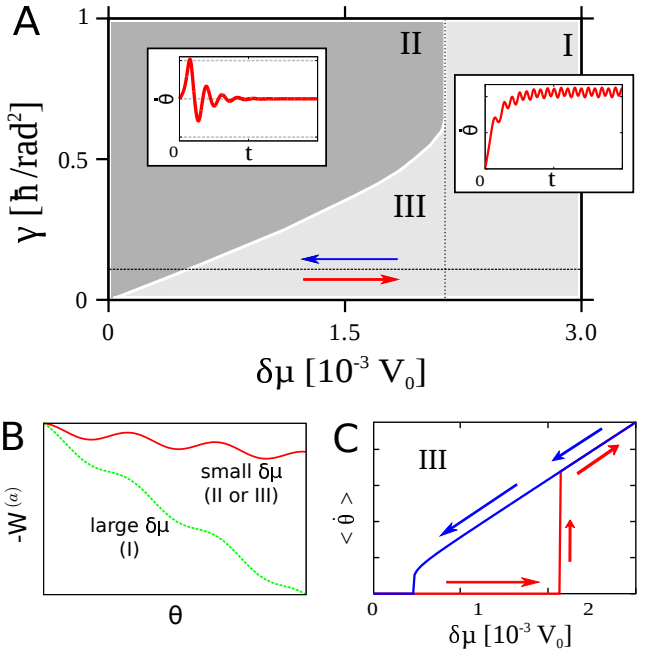

FIG. 6. **A -** Phase diagram of different steady state dynamics as function of $\delta\mu$ and γ, assumed constant for simplicity. Insets of regions I and II show typical dynamics for these regions ($\dot\theta$ vs time). The typical dynamics of region III is shown in panel C. **B -** Scheme of how $W^{(a)}(\theta)$ changes with $\delta\mu$. **C -** Average terminal velocity $< \dot\theta >$ versus $\delta\mu$ for a typical hysteresis cycle where the dynamics can fall into the cases shown in the insets of regions I or II depending on the initial conditions. The horizontal line in A marks the average value of the current induced friction coefficient, panels C was calculated with this value of γ. The vertical line in A corresponds to the value of $\delta\mu$ to which $W^{(a)}(\theta)$ vs θ does not show a minimum. $W^{(\mathrm{load})} = 0$, $\Delta = 0.001V_0$, $\epsilon = 0$, $\lambda = 25a$, and border condition "linear 25".

the low temperature limit $T \approx 0$.

As discussed in the previous subsection the system-lead mismatching introduces corrections to the CIFs and one of the consequences of this is the oscillatory behavior of $W^{(a)}(\theta)$. This effects in turn induces, under the appropriate conditions, a dependence of the final state of the system with the initial conditions. This, can be easily understood considering the following example. Suppose $W^{(\mathrm{total})}$ posses a minimum, as the case labeled "small $\delta\mu$" in panel B of fig. 6, and assume the dynamics starts from the first maximum to the left of that minimum with a temperature close to zero and with a small velocity pointing to the right. Additionally, let us assume that the energy dissipated as friction is lower than the energy gained by reaching the first maximum to the right. Under this condition the system will keep moving to the right accelerating its motion until the energy dissipated becomes so large that $W^{(\mathrm{total})} = 0$. This dynamics will look like that shown in the inset of region I of panel A of fig. 6. If, we start from the minimum under the same condition,

the system will follow a damped oscillatory dynamics as that shown in the inset of region II of panel A of fig. 6. Both described situations can be found in region III of the phase diagram of panel A of fig. 6, where the final state depends on the initial condition. Summarizing, in this region if the rotor was still, it will remain still, but if it is already rotating, it will continue to rotate.

The above mentioned effect, is not present at larger $\delta\mu$, where $W^{(a)}(\theta)$ does not present a minimum. In this case, independently of the initial condition the system will move until the stationary condition is reached, $W^{(\text{total})} = 0$, at a high enough average terminal velocity. This situation corresponds to region I of the phase diagram of panel A of fig. 6 and its typical dynamics looks like that of its correspondent inset. The other possibility is that $W^{(a)}(\theta)$ does present a minimum but γ is so large that the energy gained after one period does not compensate the energy lost as friction, even if the initial velocity is infinitesimally small. This situation corresponds to region II of the phase diagram of panel A of fig. 6. Its typical dynamics looks like that of its corespondent inset. Panel C of fig. 6 shows the average terminal velocity resulting from different dynamics calculated by varying progressively the applied voltage, first increasing the voltages from zero, lower red arrow, and then decreasing it starting from a high voltage, upper blue arrow. Note the hysteresis cycle that occurs in region III and the linear dependence of $< \dot{\theta} >$ on $\delta\mu$ which is consistent with $\dot{\theta}(\theta)$ approximately constant, see eq. 39.

The effect of a load coupled to the motor will be that of an additional friction or a constant force. The first case occurs for instance when the motor has to drag a mass against an external friction sources while the second occurs for example when the motor is lifting up a mass against gravity. In both cases the behavior of the system will be like that describe above but with either a corrected value of γ or a corrected value of $\delta\mu$ respectively.

In this section our intention was to highlight the importance of the boundary induced CIFs in the dynamics. For this reason we only discuss the zero temperature limit of the dynamics where the difference between dynamical regimes are clearer. At finite temperatures, crossing a barrier becomes just a matter of probabilities or waiting enough time. Under this condition the behaviors discussed are still present but blurred by temperature and the transitions form one regime to the other are smoother. If temperature is high enough, the dynamics looks like that of a random walk where even backward motion is allowed and the average velocity result from the difference in the probabilities of moving in one or the other direction, (see ref.[40] and references therein).

C. Effect of decoherence

In a Thouless motor, all electrons incoming to the wire with energy within the band gap are reflected. Conservation of momentum imposes that electron back-scattering should move the rotor. As transmittance is close to zero within the band gap, $I^{total} \approx I^{pump}$, Onsager's relations, eq. 25, implies that all electrons passing through the system contribute to the work per cycle. The result of this is that the efficiency goes towards one in the limit of small velocities, see eq. 37 . Since the band gap is a consequence of the quantum nature of the electrons, its is natural to wonder about the performance of the motor under dephasing environments.

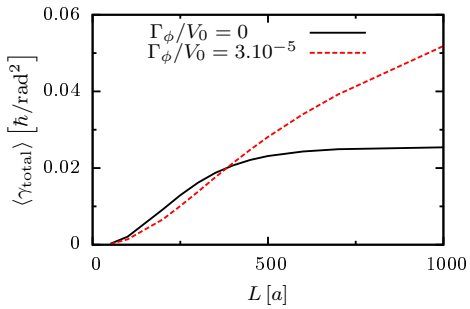

FIG. 7. Effect of decoherence and the system's length L on the averaged total friction coefficient $\langle\gamma_{\text{total}}\rangle$. $\Delta = 0.001V_0$, $\epsilon = 0$, and $\lambda = 25a$.

Let us assume that the rate to which electrons undergo decoherent events, $2\Gamma_\phi/\hbar = 1/\tau_\phi$, is constant along the wire but negligible within the leads. Then, electrons crossing a wire of total length L and decoherent length $L_\phi = 2v_f\Gamma_\phi/\hbar$ have a probability $P \propto e^{-L/L_\phi}$ of traversing the system without undergoing a decoherent event. If the total length of the system L is close to L_ϕ then it will be necessary to include the effect of decoherence on CIFs. In section II we developed the theory that allow us to do so.

Fig. 7 shows the effect of decoherence and the length of the system on the total friction coefficient $\gamma_{\text{total}} = \gamma^{eq} + \gamma^{\phi}$. First note that there is a saturation of γ_{total} at large L. This is reasonable since the Fermi energy is within the band gap and then electrons posses a penetration depth beyond which the system is not explored. This penetration depth is of course increased by decoherence which in turn increases the value of L to which γ_{total} saturates. The other interesting feature to be noticed is the change in the behavior of γ_{total} with or without decoherence for systems of different lengths. Note that for short systems decoherence always reduce the friction while for long systems is the opposite. This can be understood as two competing effects of decoherence on γ. First, the type of decoherence described by our model does preserve energy but not momentum, which in turn induced a random-walk-like dynamics of electrons, in a semiclassical picture. This phenomenon should increase the noise and then γ_{total} with Γ_ϕ. Second, for small systems adding reservoirs or increasing the connection to them, tends to reduce the noise in the currents, which on

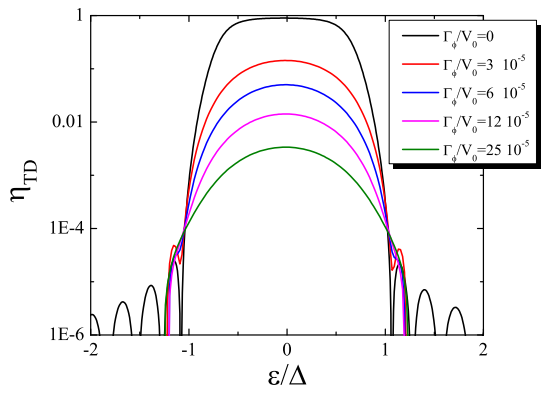

FIG. 8. Effect of decoherence on the thermodynamic efficiency η_{TD} for different values of the Fermi energy, measured from the center of the band gap. $L = 2000a$, $\Delta = 0.001V_0$, and $\lambda = 25a$. We assumed an external dissipative mechanism with $\gamma_{\rm ext} = 10^3\hbar/{\rm rad}^2$.

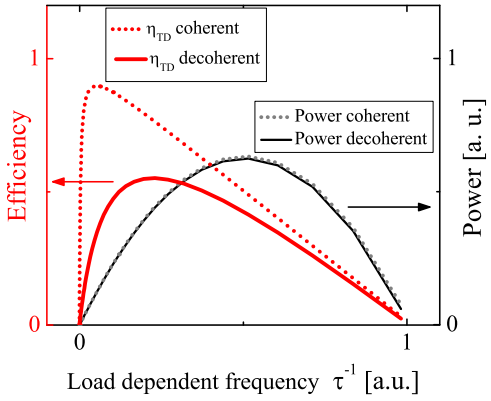

FIG. 9. Effect of decoherence on the thermodynamic efficiency η_{TD} and the output power $\dot{W}^{(\rm load)}$ (in arbitrary units) for different operational frequencies of the motor τ^{-1} (in arbitrary units). $L = 2000a$, $\Delta = 0.001V_0$, $\epsilon = 0$, and $\lambda = 25a$.

the other hand is the source of noise of CIFs.[33,41] Then it is expected for small systems a decrease of $\gamma_{\rm total}$ with Γ_ϕ. As can be seen in the figure, the first effect dominates at large (L)s while the second one dominates at small (L)s.

In the next figures, 8 and 9, we assume for simplicity that current induced frictions are much lower than other external sources of frictions and estimate the values of $\gamma_{\rm ext}$ from the experiments of reference[42], assuming also $\gamma_{\rm ext}$ independent of θ. The value used in the figures is $\gamma_{\rm ext} = 10^3\hbar/{\rm rad}^2$. In any case, the qualitative behavior of the efficiency and the output power per cycle does not depend on the particular value of γ used.

In fig. 8 we can see the efficiency for different values of Γ_ϕ/V_0. As expected, decoherence has a profound influence on the efficiency, dropping its maximum value by an order of magnitude for $\Gamma_\phi/V_0 = 3\ 10^{-5}$. To put this into context, a tight binding chain of the same length but without the periodic potential gives $L/L_\phi = 0.5$ which implies that almost half of the electrons would suffer a decoherent event while passing through the sample. It is interesting that some memory of the quantum nature of the Thouless motor remains even at high decoherent rates. Note that even for $\Gamma_\phi/V_0 = 25\ 10^{-5}$ the curves within the band gap keep a similar shape. This decoherent rate for the same system but without the periodic potential gives $L/L_\phi = 4$, which implies that only 1 out of 50 electrons would pass the system without suffering a decoherent events.

Finally, it is important to compare the efficiency η_{TD} and the output power $\dot{W}$ as function of the period of the motor τ. This is done in fig. 9. There are at least two important features to be discussed in the figure. First, the conditions that maximize η_{TD} and $\dot{W}$ do not coincide, and second the effect of decoherence on η_{TD} is much stronger than for $\dot{W}$. The first result is reasonable. Just by looking at eq. 37 it is clear that at $I^{bias} = 0$, $\tau \to \infty$ maximize η_{TD} by minimizing the energy dissipated as friction, while this condition makes $\dot{W} = W/\tau \to 0$. The consequence is that, as in the case of macroscopic engines, one has to choose between maximizing the output power or the efficiency of the motor. The second feature, η_{TD} more sensitive to decoherence than $\dot{W}$, shows that the decrease in efficiency is just a consequence of the increase of the transmittance and not of the decrease in W.

IV. CONCLUSIONS

We have extended our previous theory of decoherence in CIFs to account for multiple site-dependent decoherent processes providing analytical expressions for the CIFs, friction coefficients and self correlation functions of the forces. We have proved that our model is thermodynamically consistent, fulfilling fluctuation dissipation theorem, Onsager's reciprocity relations, and the first and the second laws of thermodynamics.

We have found that decoherence drastically reduce the efficiency of the motor mainly due to the increase in conductance, while its effect on the output power is not so important. Its effect on the current induced friction depends on the length of the system, reducing the friction for short systems while increasing it for long ones.

We have confirmed that the conditions that maximize the efficiency do not coincide with those that maximize the output power at least at low to intermediate decoherent rates

We have shown that the system-lead mismatching produce conservative forces that can dramatically alter the dynamics of Thouless motors. At high dissipation, these forces set a minimum voltage that allows the operation of the motor. At low dissipation, the boundary induced

forces cause hysteresis with two limiting voltages that switch on-off the movement of the motor depending on its previous history.

V. ACKNOWLEDGEMENT.

This work was supported by CONICET, SECYT-UNC and ANPCyT.

Appendix A: Positivity of $\mathbb{T}$, γ^{eq} and γ^{ϕ} matrices

Gauge invariance of the bias current implies that a constant shift of the chemical potentials must not yield additional currents through the system. This condition is encoded in the relation $\sum_{\beta\neq\alpha} T_{\alpha\beta} = \sum_{\beta\neq\alpha} T_{\beta\alpha}$ and force the definition $T_{\alpha\alpha} = -\sum_{\beta\neq\alpha} T_{\alpha\beta}$. This is the central property that in the end guarantees the positivity of the γ^{ϕ} and $\mathbb{T}$ matrices and in turn the positivity of the entropy production with or without decoherence, eq. 28.

The Gershgorin's circle Theorem[43] applied to our problem, $\mathbb{T}$ symmetric, establish that

$$\lambda \in \bigcup_{\alpha} D_{\alpha} \text{ where } D_{\alpha} = \left\{ x \in \mathbb{R} : |x - T_{\alpha\alpha}| \leq \sum_{\beta\neq\alpha} T_{\alpha\beta} \right\}.$$

where λ is an eigenvalue of $\mathbb{T}$. The above implies that all x in the interval D_{α} satisfies

$$-2 < T_{\alpha\alpha} - \sum_{\beta\neq\alpha} T_{\alpha\beta} \leq \ x \ \leq T_{\alpha\alpha} + \sum_{\beta\neq\alpha} T_{\alpha\beta} \leq 0,$$

Thus, in particular,

$$x \ \leq 0.$$

The union of all sets D_{α} does not contain positive values, and then $(-\mathbb{T})$ is a positive semi-definite matrix.

The positivity of the matrix γ^{ϕ} depends on that of the matrix $(-\mathbb{T}_{\phi\phi})^{-1}$. We start by first noticing that $\mathbb{T}_{\phi\phi}$ and $\mathbb{T}_{\phi\phi}^{-1}$ are symmetric for the case of interest. Then, the diagonal elements of $\mathbb{T}_{\phi\phi}$ satisfy the following condition

$$\left|[\mathbb{T}_{\phi\phi}]_{\alpha\alpha}\right| = \sum_{\beta\neq\alpha,\beta\in\ell,\phi} T_{\alpha\beta} > \sum_{\beta\neq\alpha,\beta\in\phi} T_{\alpha\beta} \qquad \text{(A1)}$$

where $T_{\alpha\alpha} < 0$, and $T_{\alpha\beta} > 0$ for $\alpha \neq \beta$. Unlike the previous case with the matrix $\mathbb{T}$, the diagonal elements of $\mathbb{T}_{\phi\phi}$ are strictly greater than $\sum_{\beta\neq\alpha,\beta\in\phi} T_{\alpha\beta}$. By applying the Gershgorin circle's theorem to this case we conclude that all λ^{ϕ}'s, eigenvalues of $\mathbb{T}_{\phi\phi}$, are strictly negative. This implies that $(-\mathbb{T}_{\phi\phi})^{-1}$ is positive definite, which ensures the positivity of the matrix γ^{ϕ}.

Given the unitarity of the S matrix, which is a consequence of particle conservation, one can readily prove that $S^{\dagger}\partial S$ is pure imaginary. Then, using the reciprocal relation for the case of interest in this work, $S_{\alpha\beta} = S_{\beta\alpha}$, and the fact that $-\partial f/\partial\varepsilon \geq 0$ one arrives to

$$\gamma^{eq}_{\nu,\nu} = \frac{1}{2}\int \frac{d\varepsilon}{2\pi}\left(-\frac{\partial f}{\partial\varepsilon}\right)\sum_{\alpha,\beta}\left|S^{\dagger}\frac{\partial S}{\partial x_{\nu}}\right|^{2}_{\alpha,\beta} \geq 0 \qquad \text{(A2)}$$

Positivity of $\vec{x}^{T}\gamma^{eq}\vec{x}$ is obvious by considering a change of basis where γ^{eq} is diagonal.

Combining the three previous results we conclude that the rate of entropy production given by eq. 28 is always greater or equal to zero, as required by Thermodynamics.

* Corresponding author: rbustos@famaf.unc.edu.ar

[1] D. Dundas, E.J. McEniry, and T.N. Todorov. Current-driven atomic waterwheels. *Nature Nanotech.*, 4:99, 2009.

[2] S. W. D. Bailey, I. Amanatidis, and C. J. Lambert. Carbon nanotube electron windmills: A novel design for nanomotors. *Phys. Rev. Lett.*, 100:256802, 2008.

[3] Tibor Kudernac, Nopporn Ruangsupapichat, Manfred Parschau, Beatriz Macia, Nathalie Katsonis, Syuzanna R. Harutyunyan, Karl-Heinz Ernst, and Ben L. Feringa. Electrically driven directional motion of a four-wheeled molecule on a metal surface. *Nature*, 479:208, 2011.

[4] Josef Michl and E. Charles H. Sykes. Molecular rotors and motors: Recent advances and future challenges. *ACS Nano*, 3:1042, 2009.

[5] Heather L Tierney, Colin J Murphy, April D Jewell, Ashleigh E Baber, Erin V Iski, Harout Y Khodaverdian, Allister F McGuire, Nikolai Klebanov, and E Charles H Sykes. Experimental demonstration of a single-molecule electric motor. *Nature nanotechnology*, 6(10):625–629, 2011.

[6] Franco Chiaravalloti, Leo Gross, Karl-Heinz Rieder, Sladjana M Stojkovic, André Gourdon, Christian Joachim, and Francesca Moresco. A rack-and-pinion device at the molecular scale. *Nature Materials*, 6(1):30–33, 2007.

[7] Harold G Craighead. Nanoelectromechanical systems. *Science*, 290(5496):1532–1535, 2000.

[8] Michael Roukes. Nanoelectromechanical systems face the future. *Physics World*, 14(2):25, 2001.

[9] Niels Bode, Silvia Viola Kusminskiy, Reinhold Egger, and Felix von Oppen. Scattering theory of current-induced forces in mesoscopic systems. *Phys. Rev. Lett.*, 107:036804, Jul 2011.

[10] Mark Thomas, Torsten Karzig, Silvia Viola-Kusminskiy, Gergely Zaránd, and Felix von Oppen. Scattering theory of adiabatic reaction forces due to out-of-equilibrium quantum environments. *Phys. Rev. B*, 86:195419, 2012.

[11] Eunan J McEniry, Tchavdar N Todorov, and Daniel Dundas. Current-assisted cooling in atomic wires. *Journal of Physics: Condensed Matter*, 21(19):195304, 2009.

[12] Liliana Arrachea, Eduardo R Mucciolo, Claudio Chamon, and Rodrigo B Capaz. Microscopic model of a phononic refrigerator. *Physical Review B*, 86(12):125424, 2012.

[13] Michael Galperin, Keiji Saito, Alexander V Balatsky, and

Abraham Nitzan. Cooling mechanisms in molecular conduction junctions. *Physical Review B*, 80(11):115427, 2009.

[14] Raúl Bustos-Marún, Gil Refael, and Felix von Oppen. Adiabatic quantum motors. *Phys. Rev. Lett.*, 111:060802, 2013.

[15] DJ Thouless. Quantization of particle transport. *Physical Review B*, 27(10):6083, 1983.

[16] X.-L. Qi and S. C. Zhang. Field-induced gap and quantized charge pumping in a nanoscale helical wire. *Phys. Rev. B*, 79:235442, 2009.

[17] Lucas J. Fernández-Alcázar, Raúl A. Bustos-Marún, and Horacio M. Pastawski. Decoherence in current induced forces: Application to adiabatic quantum motors. *Phys. Rev. B*, 92:075406, 2015.

[18] Carlos J Cattena, Lucas J Fernández-Alcázar, Raúl A Bustos-Marún, Daijiro Nozaki, and Horacio M Pastawski. Generalized multi-terminal decoherent transport: recursive algorithms and applications to saser and giant magnetoresistance. *J. Phys.: Condens. Matter*, 26(34):345304, 2014.

[19] Niels Bode, Silvia Viola Kusminskiy, Reinhold Egger, and Felix von Oppen. Current-induced forces in mesoscopic systems: A scattering-matrix approach. *J. Nanotechnol.*, 3:144, 2012.

[20] M. Büttiker. Role of quantum coherence in series resistors. *Phys. Rev. B*, 33:3020, 1986.

[21] H. M. Pastawski and E. Medina. Tight binding methods in quantum transport trough molecules and small devices: from the coherent to the decoherent description. *Rev. Mex. Fis.*, 47S1:1, 2001.

[22] Y. Imry and R. Landauer. Conductance viewed as transmission. *Rev. Mod. Phys.*, 71:S306, 1999.

[23] M. Büttiker, H. Thomas, and A. Prêtre. Current partition in multiprobe conductors in the presence of slowly oscillating external potentials. *Zeitschrift für Physik B Condensed Matter*, 94(1):133–137, 1994.

[24] P. W. Brouwer. Scattering approach to parametric pumping. *Phys. Rev. B*, 58:R10135–R10138, 1998.

[25] Elihu Abrahams, editor. See chap. 8, by Büttiker and Moskalets, of *'50 years of Anderson localization'*. World Scientific Publishing Co. Pte. Ltd., 2010.

[26] Ya. M. Blanter and M. Büttiker. Shot noise in mesoscopic conductors. *Phys. Rep.*, 336:1, 2000.

[27] H. M. Pastawski. Classical and quantum transport from generalized landauer-büttiker equations. *Phys. Rev. B*, 44:6329, 1991.

[28] H. M. Pastawski. Classical and quantum transport from generalized landauer-büttiker equations. ii. time-dependent resonant tunneling. *Phys. Rev. B*, 46:4053, 1992.

[29] N. A. Zimbovskaya and M. M. Kuklja. Vibration-induced inelastic effects in the electron transport through multisite molecular bridges. *J. Chem. Phys.*, 131:114703, 2009.

[30] Lucas J. Fernández-Alcázar and Horacio M. Pastawski. Decoherent time-dependent transport beyond the landauer-bttiker formulation: A quantum-drift alternative to quantum jumps. *Phys. Rev. A*, 91:022117, 2015.

[31] J. L. D'Amato and H. M. Pastawski. *Phys. Rev. B*, 41:7411, 1990.

[32] C. J. Cattena, R. A. Bustos-Marún, and H. M. Pastawski. Crucial role of decoherence for electronic transport in molecular wires: Polyaniline as a case study. *Phys. Rev. B*, 82:144201, 2010.

[33] CWJ Beenakker and M Büttiker. Suppression of shot noise in metallic diffusive conductors. *Phys. Rev. B*, 46(3):1889, 1992.

[34] M. Moskalets and M. Büttiker. Effect of inelastic scattering on parametric pumping. *Phys. Rev. B*, 64:201305, 2001.

[35] J. N. H. J. Cremers and P. W. Brouwer. Dephasing in a quantum pump. *Phys. Rev. B*, 65:115333, 2002.

[36] M Buttiker. Symmetry of electrical conduction. *IBM Journal of Research and Development*, 32(3):317–334, 1988.

[37] María Florencia Ludovico, Francesca Battista, Felix von Oppen, and Liliana Arrachea. Adiabatic response and quantum thermoelectrics for ac-driven quantum systems. *Phys. Rev. B*, 93:075136, 2016.

[38] Doron Cohen. Quantum pumping and dissipation: From closed to open systems. *Phy. Rev. B*, 68:R201303, 2003.

[39] María Florencia Ludovico, Michael Moskalets, David Sánchez, and Liliana Arrachea. Dynamics of energy transport and entropy production in ac-driven quantum electron systems. *Phys. Rev. B*, 94:035436, 2016.

[40] Peter Hänggi and Fabio Marchesoni. Artificial brownian motors: Controlling transport on the nanoscale. *Rev. Mod. Phys.*, 81:387–442, 2009.

[41] R. C. Liu and Y. Yamamoto. Nyquist noise in the transition from mesoscopic to macroscopic transport. *Phys. Rev. B*, 50:17411, 1994.

[42] John Cumings and A Zettl. Low-friction nanoscale linear bearing realized from multiwall carbon nanotubes. *Science*, 289(5479):602–604, 2000.

[43] David Kincaid and Ward Cheney. *Numerical analysis sathematics of scientific computing, Second Edition.* Brooks/Cole Publishing Company, 1991.